Spatial and Time Patterns Extraction of Eddy Current Pulsed Thermography Using Blind Source Separation

Libing Bai, Bin Gao, *Member, IEEE*, Gui Yun Tian, *Senior Member, IEEE*, Wai Lok Woo, *Senior Member, IEEE*, and Yuhua Cheng, *Member, IEEE*

***Abstract*— Eddy current pulsed thermography (ECPT), a new emerging nondestructive testing and evaluation (NDT&E) technique, has been applied for a wide range of conductive materials. The acquired image sequences contain valuable information in both spatial and time domain. ECPT techniques mainly use a specific frame to detect and quantify the defects. However, selection of specific frame from transient thermal image video to maximize the contrast of thermal variation and defect pattern from complex geometrical samples remain a challenge. In order to accurately find anomalous patterns from the transient thermal pattern for defect detection and further quantitative NDE, this paper employs a single channel blind source separation algorithm. This method enables spatial and time patterns to be extracted according to the whole transient response behavior without any training knowledge. In this paper, both mathematical and physical models are discussed, and the basis of the proper selection of contrast image is given. In addition, the artificial slot and thermal fatigue natural crack are applied to validate the proposed method.**

***Index Terms*— Blind source separation, eddy current pulsed thermography, nondestructive evaluation, pattern extraction.**

I. Introduction

THE major advantage of thermography over other techniques is the potential in accurate noncontact inspection of a large area within a short time and large standoff distances [1]. A review of current literature shows that thermography is applicable to a wide range of materials, including glass fiber reinforced polymer specimen [2], carbon fiber reinforced polymer composites [3], power electronic devices [4] and steel [5] with great success. Eddy Current Pulsed Thermography (ECPT), named Pulsed Eddy Current (PEC) thermography in previous works, is a new emerging Nondestructive Testing and Evaluation (NDT&E) technique, which combines two techniques, Eddy Current (EC) and thermography [6]. In test phase, a high-current electromagnetic pulse is employed to induce eddy current in the conductive material under inspection for a short period (typically less than 1s). The resultant surface heat distribution from Joule heating and heat diffusion procedure is recorded using an infrared camera for the detection of discontinuities.

ECPT has been attempted in previous studies. The temperature distribution around a crack with different penetration depths in metallic materials was investigated in [7]. The potential for small defects detection in components of complex geometry such as compressor blades, low pressure turbine vanes was discussed in [8]. The probability of detection (POD) of fatigue cracks in steel, titanium and nickel-based superalloy was estimated in [9]. Multiple cracks from rolling contact fatigue in rail track in a single measurement were detected in [10]. The wealth of information of ECPT transient pattern has attracted a wide interest. Several transient response features have been used for quantification of defect, which is critical for acceptance/rejection decisions for maintenance and lifetime prediction. Two detections modes (transmission mode and reflection mode) for wall thinning and inner defects characterisation using time to peak were compared in [11]. ECPT was employed for steel stress characterisation using peak value [12]. Notches in carbon fiber reinforced plastic material through analysis of the surface heating pattern were evaluated. It demonstrated that a deeper notch results in a faster normalized temperature decay rate in the cooling phase; a narrower notch leads to a faster temperature rise and decay rate at the beginning of the heating phase and in the cooling phase, respectively; and the notch locations with respect to the coil does not change the normalized transient response [13].

All the above works are limited by the manual selection of proper contrast frames. In addition, the transient response features suffer from noise. To enhance the flaw contrast and improve noise rejection qualities, pattern based image enhancement has been conducted by introducing the raw data upon a set of orthogonal basis functions. Fourier

Manuscript received January 15, 2013; accepted January 7, 2013. Date of publication February 25, 2013; date of current version April 17, 2013. This work was supported by the University of Electronic Science and Technology of China and Newcastle University, EPSRC (EP/E005071/1), the EPSRC grant - Future reliable renewable energy conversion systems and networks: A collaborative U.K.-China Project (EP/F06151X/1), and the National Natural Science Foundation of China under Grant 61102141. The associate editor coordinating the review of this paper and approving it for publication was Prof. Okyay Kaynak. L. Bai and B. Gao contributed equally to this work. *(Corresponding author: Bin Gao.)*

L. Bai, B. Gao, and G. Y. Tian are with the School of Automation Engineering, University of Electronic Science and Technology of China, Chengdu 611731, China, and also with the School of Electrical and Electronic Engineering, Newcastle University, Newcastle upon Tyne NE1 7RU, U.K. (e-mail: libing.bai@ncl.ac.uk; bin.gao@ncl.ac.uk; g.y.tian@ncl.ac.uk).

W. L. Woo is with the School of Electrical and Electronic Engineering, Newcastle University, Newcastle upon Tyne NE1 7RU, U.K. (e-mail: lok.woo@ncl.ac.uk).

Y. Cheng is with the School of Automation Engineering, University of Electronic Science and Technology of China, Chengdu 611731, China (e-mail: yhcheng@uestc.edu.cn).

Color versions of one or more of the figures in this paper are available online at http://ieeexplore.ieee.org.

Digital Object Identifier 10.1109/JSEN.2013.2248931

transform was applied to pulsed thermography, and enhanced the flaw-contrast significantly using phase map [14]. Influence of nonuniform heating and surface emissivity variation was removed by using a Fourier transformation based image reconstruction algorithm [15]. Instead of a prescribed set of basis functions, empirical orthogonal functions were also employed to maximize the anomalous patterns of transient response. The efficiency of Principal Component Analysis (PCA) was compared on thermography features extraction by considering the initial sequence as either a set of images or a set of temporal profiles [16]. Water leakage was identified in dikes from thermometric data using PCA and Independent Component Analysis (ICA) [17]. Rajic employed Principal Component Analysis (PCA) to improve the flaw detectivity of thermography, and characterized the surface flaw depth using characteristic time estimated from Principle Component (PC) vector [18].

However, all mentioned works only employ the source separation methods as a signal processing tool. The mathematical reasons why these algorithms can enhance an image and how these techniques are connected to physical models are not provided in detail. The results are acceptable but generally not predictable. The proper contrast components have to be empirically selected. This ambiguous case prevents the use of ECPT in automated environments. In this paper, a single channel blind source separation method is developed to extract anomalous patterns from transient thermal videos. This method can automatically highlight the defects in the spatial components and the time components. The basis of the anomalous image identification is also given, which is a first step towards the automation of defect identification. Experimental tests on man-made metal slots and natural defects with complex geometry have been conducted which shows the validation of pattern extraction.

The rest of the paper is organized as follows: section II discusses the implementation of source separation method in ECPT through an example of artificial slot detection; section III introduces the experimental set-up; section IV and V present the experiment results and the conclusions.

II. Theoretical Considerations

A. Mixing Model

During ECPT testing, when eddy current encounter a discontinuity e.g. a slot or notch, they are forced to divert, leading to areas of increased and decreased eddy current density and resultant hot and cool area due to Joule heating. In this paper, a finite in length but extending completely through the sample slot is considered as an instant to verify the proposed method, as shown in Fig. 1c. The resultant heating frame from ECPT is presented in Fig. 1. In the heating phase, different heat generation rates enlarge the temperature spatial variation. Hot spots are observed around the slot tips and the cool areas locate at both sides of the slot Fig. 1(a) [20], [21]. In the cooling phase, heat diffused from high temperature area to low temperature area, and reduces the contrast (Fig. 1b). This can be described using different transient responses from different positions as shown in Fig. 1 (d) (More details will be described

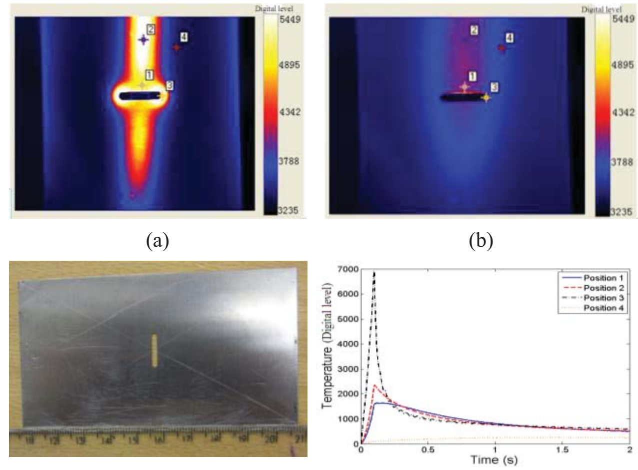

(a) (b) (c) (d)

Fig. 1. (a) Temperature distribution at 0.1 s. (b) Temperature distribution at 1.27 s. (c) Steel sample with slot. (d) Transient responses of different positions.

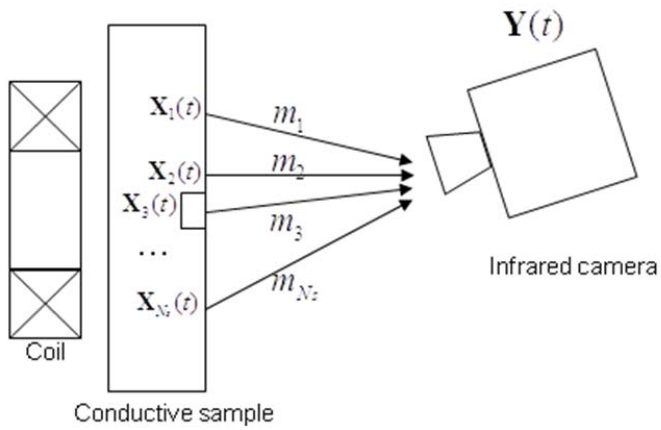

Fig. 2. Schematic diagram of single channel blind source separation model for ECPT.

in Section IV). To avoid the influences of arbitrary selection of image frame from the transient thermal videos, anomalous pattern extraction is investigated in this paper.

These different transient responses shown in Fig. 1(d) can be considered as independent signals corresponding to different areas. In specific terms, position 1 represents an area with high rising rate followed by an effectively constant temperature (0.1s) and then decay; position 2 represents an area with moderate rising and falling rate; position 3 represents an area with high rising and high falling rate of temperature; and position 4 represents an area with continually increasing temperature.

The schematic diagram of ECPT is presented in Fig. 2. The thermography image captured by the infrared camera is considered as a mixing observation $\mathbf{Y}(t)$. $\mathrm{m_i}$, $(i = 1, 2, 3, \ldots, N_s)$ is the mixing vector which describes the contribution of the i^{th} position to the recorded thermography image. N_s denotes the number of independent signal images.

As there is only one observation (infrared camera) in ECPT, this refers to a typical single channel source separation

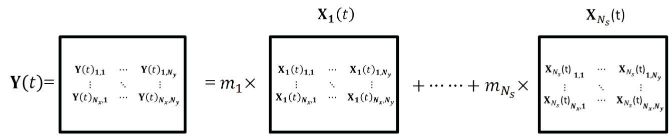

Fig. 3. Mathematic form of mixing process of ECPT.

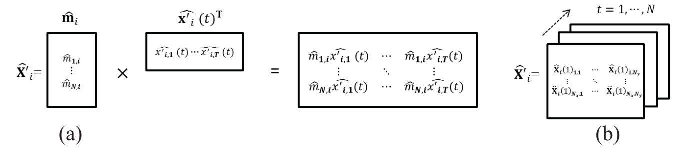

Fig. 5. (a) Visual explanation of (7). (b) Tensor representation of $\widehat{\mathbf{X}}'_i$.

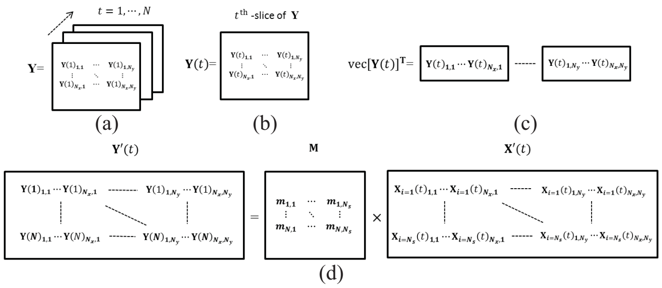

Fig. 4. (a) Tensor representation of the image sequences $\mathbf{Y}$. (b) t^{th} frame of $\mathbf{Y}$. (c) Visual explanation of $\text{vec}(\mathbf{Y}(t))^T$. (d) Visual explanation of (2).

problem [23], [24]. Figs. 3, 4, and 5 denote the mathematic form of ECPT, tensor representation and its expansions, reconstruction form, respectively. Assuming the mixing procedure follows the linear instantaneous mixing model, and the mathematical model can be described as:

$$\mathbf{Y}(t) = \sum_{i=1}^{N_s} m_i \mathbf{X}_i(t) \tag{1}$$

Then, the visual representation of Eq. (1) can be shown as where $\mathbf{Y}(t)$ and $\mathbf{X}_i(t)$ denote the recorded image and the independent image signal generated by the area of position i at time t with dimensional N_x by N_y, respectively. In this study, N_x by N_y are defined by the infrared camera sensor array with setting as $N_x = 256$, $N_y = 320$. Eq. (1) is the special case of instantaneous underdetermined BSS problem where $N_o = 1$ ($N_o << N_s, N_o$ denotes the number of recorded image), is termed as single channel blind source separation (SCBSS) [22]. In this model, it is difficult to directly apply conventional BSS (e.g. ICA) method to separate the mixture where this method yields good performances only if the number of observed signals is equal or more than the number of independent sources.

B. Single Channel Blind Source Separation

To solve above ill-posed problem ($N_o << N_s$), we adopt a decomposition-based approach as another generative model. This approach was employed formerly in analyzing non-stationary sources [23], [24] by expressing a fixed-length segment drawn from transient response, such that continuous transient slices of length N can be chopped out of a set of image sequences from t to $t + N - 1$, and the subsequent segment is denoted as equivalent as image sequences captured by N independent infrared cameras $\mathbf{Y}'(t) = [\text{vec}(\mathbf{Y}(t)), \text{vec}(\mathbf{Y}(t+1)), \ldots, \text{vec}(\mathbf{Y}(t+N-1))]^T$ where 'T' denotes transpose operator and 'vec' denotes the vectorization operator. The constructed image sequence is then expressed as a linear combination of the signals generated by the independent areas such that

$$\mathbf{Y}'(t) = \mathbf{M}\mathbf{X}'(t) \tag{2}$$

where mixing matrix $\mathbf{M} = [\mathbf{m}_1, \ldots, \mathbf{m}_{N_s}]$ and $\mathbf{m}_i$ is the i^{th} mixing vector. The visual representation of Eq. (2) can be shown as follow where $\mathbf{X}'(t) = [\text{vec}(\mathbf{X}_1(t)), \text{vec}(\mathbf{X}_2(t)), \ldots, \text{vec}(\mathbf{X}_{N_s}(t))]^{\mathbf{T}}$. Assuming that $N_s = N$ and $\mathbf{M}$ has full rank so that the transforms between $\mathbf{Y}'(t)$ and $\mathbf{X}'(t)$ be reversible in both directions such that we can find the inverse matrix $\mathbf{W} = \mathbf{M}^{-1}$ which refers to the ICA method. The purpose of this decomposition is to model the multivariate distribution of $\mathbf{Y}'(t)$ in a statistically efficient manner. The ICA learning algorithm is equivalent to searching for the linear transformation that make the components as statistically independent as possible, as well as maximizing the marginal densities of the transformed coordinates for the given training data, namely

$$\widehat{\mathbf{W}} = \arg\max_{\mathbf{W}} \prod_t \Pr\left(\mathbf{Y}'(t)\middle|\,\mathbf{W}\right) = \arg\max_{\mathbf{W}} \prod_t \prod_i \Pr\left(\mathbf{x}'_i(t)\right) \tag{3}$$

where $\mathbf{x}'_i(t) = \text{vec}(\mathbf{X}_i(t))$ and $\Pr(\bullet)$ is the probability. To solve Eq. (3), we first apply PCA whiten by $\mathbf{Y}'(t)$ which is implemented here by exploiting singular value decomposition (SVD) [25] which is a factorization of the form

$$\mathbf{Y}'(t)^{\mathbf{T}} = \mathbf{U}_{T\times T}\mathbf{D}_{T\times N} \times \mathbf{V}^{\mathbf{T}}_{N\times N} \tag{4}$$

where $T = N_x \times N_y$, $\mathbf{U}_{T\times T}$ and $\mathbf{v}_{N\times N}$ are the orthogonal matrices and $\mathbf{D}_{T\times N}$ consist of the singular values. The columns of $\mathbf{U}_{T\times T}$ represent the PCA basis vectors. With possible dimension reduction, e.g. choosing $N_s \leq N$, there exits N_s number of basis vectors maximally informative subspace of input data, thus the $\mathbf{U}_{T\times N_s}$ basis vectors are selected and determined by the information contained in the nonzero singular values. The basis vectors obtained by PCA are only uncorrelated but not statistically independent. In the second stage, the independent basis vectors must be derived by employing ICA algorithm where the PCA basis vectors $\mathbf{U}_{T\times N_s}$ are considered as the observations in ICA, namely

$$\mathbf{U}^{\mathbf{T}}_{T\times N_s} = \mathbf{M}_{N_s\times N_s}\mathbf{X}'_{N_s\times T}(t) \tag{5}$$

ICA estimates the separating or demixng matrix $\widehat{\mathbf{W}}$ that is an approximation of the inverse of the original mixing matrix $\mathbf{M}$, and obtain the independent component which can be estimated by using FastICA [19]. The independent signal can be obtained

$$\widehat{\mathbf{X}}'_{N_s\times T}(t) = \widehat{\mathbf{W}}_{N_s\times N_s}\mathbf{U}^{\mathbf{T}}_{T\times N_s} \tag{6}$$

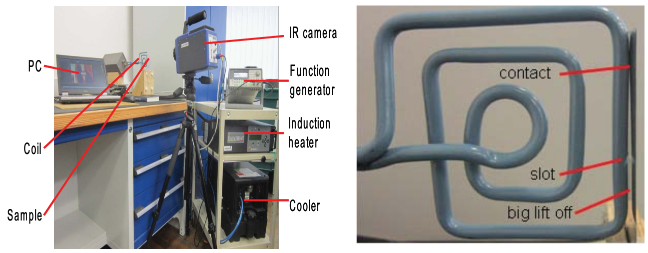

(a) (b)

Fig. 6. (a) Experiment set-up. (b) Lift-off variation between coil and sample.

For each estimated independent signal, it is interesting to find out the procedure of transient response cross time point where $t = \mathbf{1}, \ldots, N$. Thus, the reconstruction process of the independent signal image sequences generated by the i^{th} area can be expressed as

$$\widehat{\mathbf{X}}'_i = \widehat{\mathbf{m}}_i \widehat{\mathbf{x}}'_i(t)^{\mathbf{T}} \tag{7}$$

where $\widehat{\mathbf{m}}_i$ is the i^{th} vector of estimated mixing matrix $\widehat{\mathbf{M}}$, here $\widehat{\mathbf{M}} = \widehat{\mathbf{W}}^{\dagger}$ where '†' denotes the pseudo inverse where $\widehat{\mathbf{M}}$ with the dimension of N by N_s and $\widehat{\mathbf{x}}'_i(t)^{\mathbf{T}}$ denotes the i^{th} row vector of the estimated independent image $\widehat{\mathbf{X}}'_{N_s \times T}(t)$.

To validate the algorithm above, the man-made slot in Fig. 1 and natural defects on complex geometrical samples (turbine blade) are tested and discussed in the following sections.

III. Experiment Setup

The experimental set-up is shown in Fig. 6 (a). An Easyheat 224 from Cheltenham Induction Heating is used for coil excitation. The Easyheat has a maximum excitation power of 2.4 kW, a maximum current of 400 A_{rms} and an excitation frequency range of 150–400 kHz (380 A_{rms} and 256 kHz are used in this study). The system has a quoted rise time (from the start of the heating period to full power) of 5ms, which was verified experimentally. Water cooling of coil is implemented to counteract direct heating of the coil.

The IR camera, SC7500 is a Stirling cooled camera with a 320 × 256 array of 1.5–5μm InSb detectors. This camera has a sensitivity of < 20 mK and a maximum full frame rate of 383 Hz, with the option to increase frame rate with windowing of the image. A rectangular coil is constructed to apply directional excitation. This coil is made of inner diameter 6.35 mm high conductivity hollow copper tube. In the experiment, only one edge of the rectangular coil is used to stimulate eddy current to the underneath sample. In this study, the frame rate is 383 Hz, and 2 s videos are recorded in the experiments.A steel sample (0.24 mm×45 mm×100 mm) with a slot of 10 mm length, 2 mm width is prepared (Fig. 1c). A 100 ms heating duration is selected for inspection, which is long enough to elicit an observable heat pattern. To simulate the lift-off variation in complex geometrical sample test, the steel sample is placed with a small angle against the coil, as shown in Fig. 6 (b). The coil is perpendicular to the slot and across the slot centre.

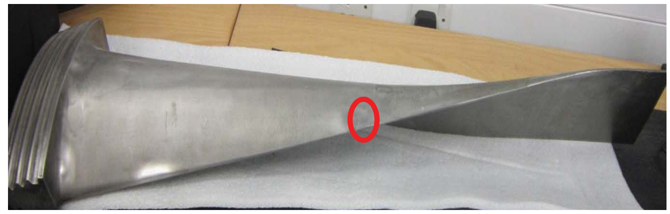

Fig. 7. Steel blade with thermal fatigue natural cracks.

A steel blade sample provided by Alstom, as illustrated in Fig. 7, where the cracks have been intentionally introduced for the purpose of the Thermography study, is also investigated for validation of the proposed method. In the blade, flaws are produced in-situ with controlled thermal fatigue loading. The flaws grow with natural thermal fatigue damage mechanism. In this study, one natural crack: 167BBB1361 is detected. The crack location is marked with red circles in Fig. 7. Crack 167BBB1361 is 4.2 mm long and coupled with a secondary crack. A 200 ms heating duration is selected for inspection.

IV. Results and Discussion

The single blind source separation method described in section II is applied for processing the recorded image sequences. After using PCA for whitening, It is possible to have dimension reduction, e.g. choosing $N_s \leq N$, there exits N_s basis vectors, which provide a subspace of data that is maximally informative, thus the $\mathbf{U}_{T \times N_s}$ basis vectors are selected and determined by the information contained in the nonzero singular values in $\mathbf{D}_{T \times N}$. Thus, we define a threshold for selected PCs which the sum of the nonzero singular values divide the sum of all PC nonzero singular values should be $\mathbf{P} \geq 99\%$. This can be calculated, namely,

$$P = \frac{\sum_{i=1}^{N_s} d_i}{\sum_{i=1}^{N} d_i} \times 100\% \tag{8}$$

where d_i corresponds to nonzero singular values in $\mathbf{D}_{T \times N}$. In our experiments the first four PC are chosen where these components already account for 99.4% of the whole singular values.

Fig. 8 shows the results by setting the number N_s of independent area equal to four. The four ICs highlight 4 complementary areas (as shown in Fig. 1), respectively: IC 1 highlights the area including position 1; IC 2 highlights the area including position 2; IC 3 highlights the area including position 3; IC 4 highlights the area including position 4. According to the central limit theorem [27], a sum of independent random variables is more Gaussian than the original variables. Thus, to uncover the independent sources, $\widehat{\mathbf{W}}$ must maximize the nongaussianity of each source. This theorem guarantees all extracted Independent Components (ICs) have their own prominent characteristics and they are not randomness. The estimated independent image $\widehat{\mathbf{x}}'_i(t)$ in Eq. (9) characterizes the amplitude distribution (spatial pattern). To

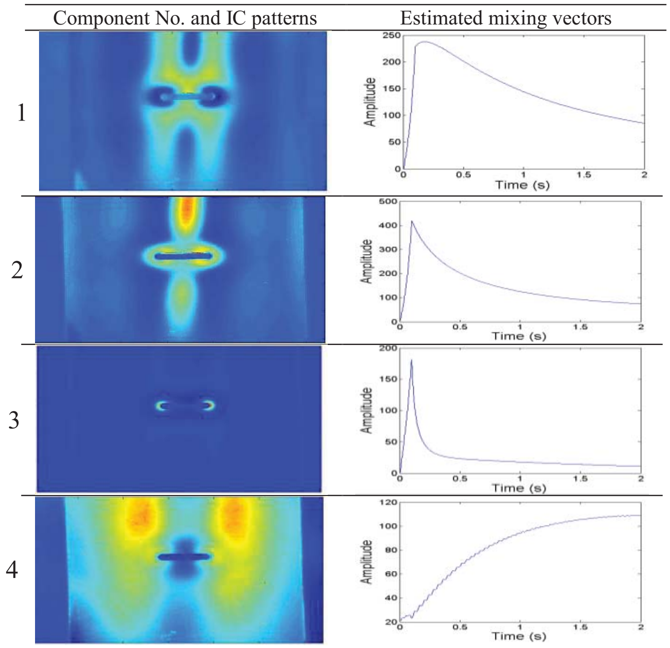

Fig. 8. Independent components and estimated mixing vectors of artificial crack.

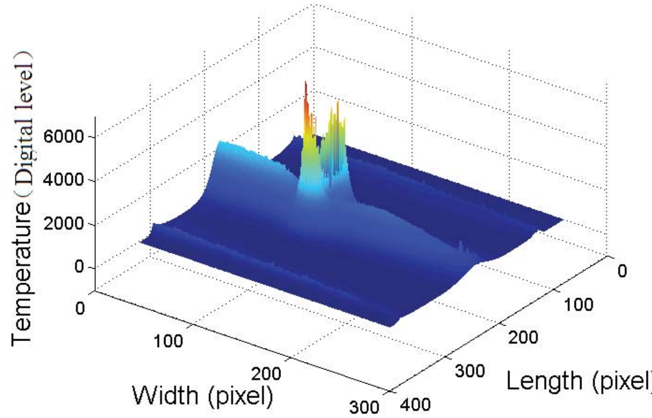

Fig. 9. Temperature distribution at the beginning of cooling phase.

verify this, the different transient patterns corresponding to these four areas are discussed below.

IC 3 highlights the singular pattern around the crack tips. In the heating phase, For a finite uniform thickness plate, a heat generation rate Q is defined as the generated heat in unite time due to Joule heating, using the Cartesian coordinates (x, y)

$$Q = \sigma \left\{ \left(\frac{\partial \phi}{\partial x} \right)^2 + \left(\frac{\partial \phi}{\partial y} \right)^2 \right\} \tag{9}$$

where ϕ denotes the electric potential, and σ electric conductivity. Since the two components of the electric current are expressed in terms of the derivatives of ϕ, heat generation rate Q theoretically goes to infinity at the crack tips. A resultant high temperature rising rate is generated in heating phase (position 3 in Fig. 1a) [26]. In the cooling phase, since there is not heating source, the variation of temperature T_{emp} in a finite uniform thickness plate is described by

$$\frac{\partial T_{emp}}{\partial t} = \frac{k}{\rho C_p} \left(\frac{\partial^2 T_{emp}}{\partial x^2} + \frac{\partial^2 T_{emp}}{\partial y^2} \right) \tag{10}$$

where t, ρ, C_p and k denotes time, mass density, heat capacity, and thermal conductivity, respectively. It is clear that the temporal variation of temperature depends on the spatial temperature variation. Fourier's law of heat conduction states that the time rate of heat transfer through a material is proportional to the negative gradient in the temperature and to the cross section area of the material. For a uniform thickness plate used in this study, the cross section area is constant. Due to the singular areas around the slot tips, a high temperature gradient is generated at the end of heating phase, as shown in Fig. 9. Therefore, a high falling rate is observed at the early stage of the cooling phase. The curve of position 3 in Fig. 1 (d) shows the transient response around slot tip, and the high rising and falling rate in heating and cooling phase is in line with the above analysis.

While high eddy current density appears around the slot tips, eddy currents are forced to spread out and results in lower EC density at either side of the slot. As a result, the temperature rising rate in the heating phase is lower than the area underneath the coil. After the period of eddy current heating, the slot affects the heat diffusion in the cooling phase. Because position 1 (at the side of the slot) is surrounded by high temperature areas (slot tips, the area underneath coil), the heat continually penetrates from the surrounding area to position 1. As a result, the slowest falling rate appears at position 1, in case the temperature continually rises at the beginning of the cooling phase. The corresponding pattern is highlighted in IC 1.

Compare to the area around crack tips, the area underneath the coil has a continual material distribution; compare to the area located at the side of the slots, the area underneath the coil has a higher eddy current density. Therefore, the heat generation rate in the heating period and temperature gradient at the early stage of cooling phase is moderate. Consequently, a moderate rising and cooling rate in the heating phase and cooling phase are generated (curve of position 2 in Fig. 1 (d)). This pattern is highlighted in IC 2.

The coil is placed in the middle along the central vertical line. Because the electromagnetic field in the material is inversely proportional to the distance between the coil and the sample, the temperature decreases from top to bottom with increasing lift-off as shown in IC 1, IC 2 and IC 4. In addition, the eddy current is negligible in the regions far from the coil (position 4 in Fig. 1a), and consequently, no inductive heating is involved. Thus, the heat diffusion from the high temperature areas (the central vertical line) dominates the thermal pattern and a continuous temperature rising is observed (curve of position 4 in Fig. 2). The area with this pattern is highlighted in IC 4.

Once four anomalous spatial patterns are extracted from the image sequences, the analysis of temperature variation behaviors corresponds to these patterns are: 1) hot area around slot tips has a high rising rate in the heating phase and high

TABLE I
CORRELATION COEFFICIENTS BETWEEN THE ESTIMATED MIXING VECTORS AND TRANSIENT RESPONSES

IC No. \ Position	1	2	3	4
1	**0.997**	0.724	0.501	0.682
2	0.720	**0.998**	0.950	0.753
3	0.410	0.900	**0.988**	0.559
4	0.706	0.774	0.692	**0.995**

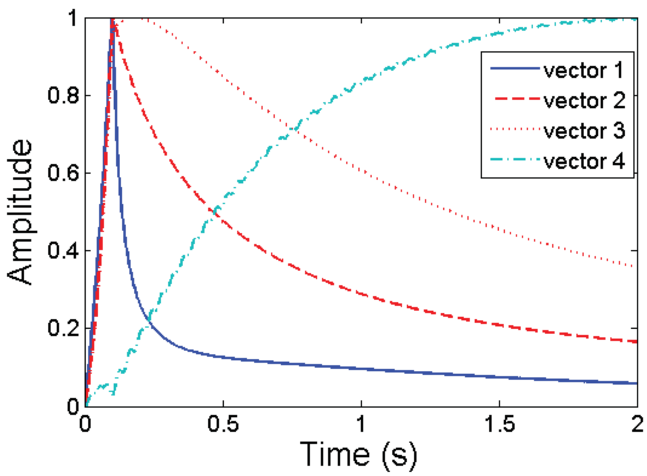

Fig. 10. Normalized estimated mixing vectors from slot.

falling rate at the beginning of cooling phase; 2) cool area at both sides of the slot has low rising rate in the heating phase and low falling rate in the heating phase; 3) the sound area has a moderate rising and falling rate in the heating and cooling phase respectively; 4) finally, a continually rising temperature in the area without inductive heating. Eq. (7) hypothesizes that the estimated mixing vectors $\widehat{\mathbf{m}}_i$ contain the transient behavior. To verify this, four estimated mixing vector 1, 2, 3, 4 are shown coupled with ICs in Fig. 8. They are similar to the transient response of position 1, 2, 3, 4 as shown in Fig. 1 (d), respectively. The correlation coefficients between these vectors and transient responses are calculated and listed in Table I. The correlation coefficients between the estimated mixing vectors and their corresponding transient responses approximate to 1 which means they are highly correlated. Specifically, the areas of four positions (Fig. 1) are highlighted by the related ICs. Therefore, the estimated mixing vectors can be used to describe the transient response patterns of the highlighted areas. In order to visualize the differences, the estimated mixing vectors are normalized and shown in Fig. 10. It is noted that the first one has the highest rising rate in the heating phase and the highest falling rate in the cooling phase which directly indicates the transient response behavior of defect area. The heat distribution for real world surface-open defects can be considered as the combination of the two fundamental defects: a notch; infinite in length, but finite in depth and a slot; finite in length but extending completely through the thickness [20], [21]. Thus, the defects can be detected by using the hot spot at the tips [26], [27].

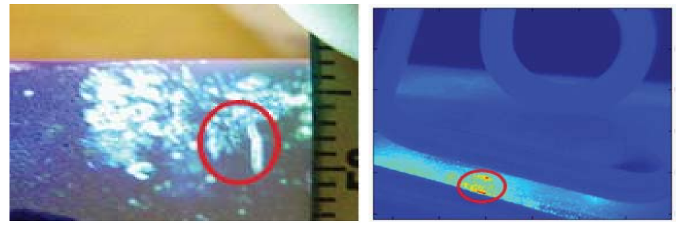

(a) (b)

Fig. 11. Thermal fatigue natural cracks detection: length: 4.2 mm and one secondary crack on the left: (a) PT image and (b) ECPT image at 0.1 s.

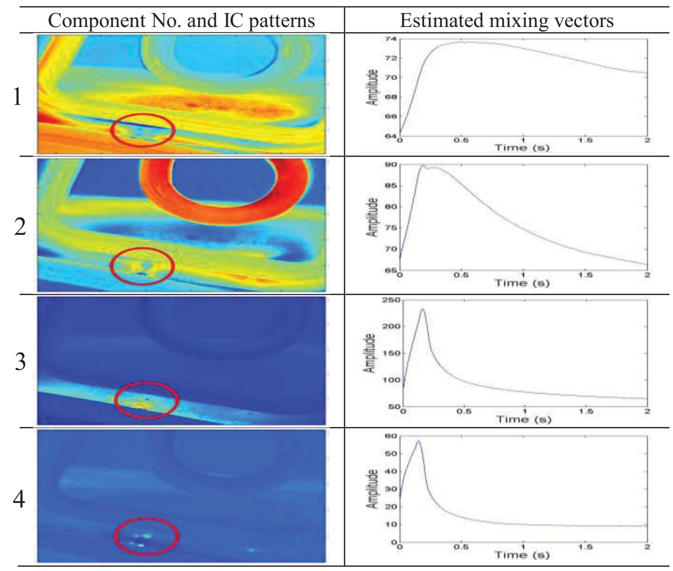

Fig. 12. Independent components and mixing vectors of natural cracks.

Since there is a singular area around the slot tips, which has a high rising and falling rate in heating and cooling phase, respectively, the defects can be highlighted by the independent component corresponding to the estimated mixing vector with high rising and falling rate (component No. 3 in Fig. 8).

To further verify above assumption, two thermal fatigue cracks (a 4.2 mm long crack coupled with a secondary crack on the left) in steel blade are employed for testing. Fig. 11 shows the Penetrant Test (PT) image provided by Alstom and ECPT image at 0.1 s. In the PT image, the area of cracks is marked with red circle. The big crack can be visually identified, while the secondary one is blurred. In the ECPT image, two hot spots are shown. This phenomenon indicates that there exist cracks in the sample. However, the cracks are difficult to be quantified.

Fig. 12 shows the results processed using single channel blind source separation method [23], [24]. It is noted that IC 1 and IC 2 highlight different parts of the excitation coil and several relative areas due to reflection of the shining sample surface. Since the heat behavior of the coil is not the target in this paper, the following analysis only concentrates on IC 3, IC 4 and their corresponding estimated mixing vectors.

IC 3 highlights the defect free area, while IC 4 highlights the 4 tips of the two cracks: two big ones on the right correspond to the tips of the big crack, and two small ones corresponds

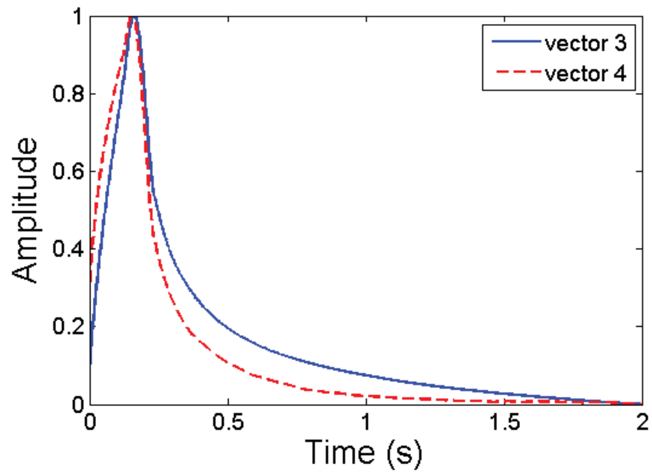

Fig. 13. Normalized estimated mixing vectors from turbine blade.

to the tips of the secondary crack on the left. Compare to the lateral heat diffusion in the thin steel sample, the heat diffuses in three dimensions in the turbine blade. Due to skin depth, the inductive heat distributes in the near surface area, and generates high temperature gradient between the surface and internal area in the heating phase. Therefore, high falling rate is extracted in both of estimated mixing vectors 3 and 4. However, there exist singular areas around the tips of cracks, a relative high rising rate in the heating phase and lower falling rate is observed in the estimated mixing vector 3, as shown in Fig. 13. The two estimated mixing vectors are normalized to highlight the difference of time patterns.

V. Conclusion

In this paper, a single channel blind source separation method is proposed for ECPT image processing. Anomalous pattern extraction from transient thermal images is proposed and discussed using man-made and natural defects. The conclusions can be drawn as follows:

1) The proposed method has highlighted the anomalous patterns of ECPT. The ICs present the spatial patterns corresponding to the eddy current and temperature distribution, while the estimated mixing vectors describe the transient behavior (time pattern).
2) The surface open cracks have been highlighted by the IC which corresponds to the estimated mixing vector with high rising rate in the heating period and high falling rate at the beginning of cooling phase around crack tips. This finding can be further used as a reference for automatically identifying the cracks from the extracted time and spatial patterns.

Future work will focus on samples with complex surface condition, e.g. roughness and emissivity variation. Complexity defects detection, e.g. subsurface defect in metallic material, impact damage and delamination in carbon fiber structures will also be investigated.

Acknowledgment

The authors would like to thank to Dr. D.-S.-S. Fernando from Alstom for providing the turbine blade and PT images.

References

[1] N. P. Avdelidis, B. C. Hawtin, and D. P. Almond, "Transient thermography in the assessment of defects of aircraft composites," *J. NDT & E Int.*, vol. 36, no. 6, pp. 433–439, 2003.

[2] Z. Zhi, T. Ning, L. Feng, and C. Zhang, "Specified value based defect depth prediction using pulsed thermography," *J. Appl. Phys.*, vol. 112, no. 2, pp. 023112-1–023112-7, Jul. 2012.

[3] C. Meola, "Nondestructive evaluation of materials with rear heating lock-in thermography," *IEEE Sensors J.*, vol. 7, no. 10, pp. 1388–1389, Oct. 2007.

[4] S. Huth, O. Breitenstein, A. Huber, and U. Lambert, "Localization of gate oxide integrity defects in silicon metal-oxide-semiconductor structures with lock-in IR thermography," *J. Appl. Phys.*, vol. 88, no. 7, pp. 4000–4003, Jul. 2000.

[5] V. S. Ghali, N. Jonnalagadda, and R. Mulaveesala, " Three-dimensional pulse compression for infrared nondestructive testing," *IEEE Sensors J.*, vol. 9, no. 7, pp. 832–833, Jul. 2009.

[6] N. Biju, N. Ganesan, C. V. Krishnamurthy, and K. Balasubramaniam, "Simultaneous estimation of electrical and thermal properties of isotropic material from the tone-burst eddy current thermography (TBET) time-temperature data," *IEEE Trans. Magn.*, vol. 47, no. 9, pp. 2213–2219, Sep. 2011.

[7] B. Oswald-Tranta and G. Wally, "Thermo-inductive surface crack detection in metallic materials," in *Proc. 9th Eur. Conf. NDT*, 2006, pp. 1–8.

[8] G. Zenzinger, J. Bamberg, W. Satzger, and V. Carl, "Thermographic crack detection by eddy current excitation," *Nondestruct. Test. Evaluat.*, vol. 22, nos. 2–3, pp. 101–111, Aug. 2007.

[9] B. Weekes, D. P. Almond, P. Gawley, and T. Barden, "Eddy-current induced thermography-probability of detection study of small fatigue cracks in steel, titanium and nickel-based superalloy," *NDT & E Int.*, vol. 49, pp. 47–56, Jul. 2012.

[10] J. Wilson, G. Y. Tian, I. Mukriz, and D. Almond, "PEC thermography for imaging multiple cracks from rolling contact fatigue," *NDT & E Int.*, vol. 44, no. 6, pp. 505–512, Oct. 2011.

[11] Y. He, M. Pan, and F. Luo, "Defect characterisation based on heat diffusion using induction thermography testing," *Rev. Sci. Instrum.*, vol. 83, no. 10, pp. 104702-1–104702-10, Oct. 2012.

[12] L. Bai and G. Y. Tian, "Stress measurement by pulsed thermography using eddy current heating," in *Proc. 51st Annu. Conf.*, 2012, pp. 1–12.

[13] L. Cheng and G. Y. Tian, "Surface crack detection for carbon fiber reinforced plastic (CFRP) materials using pulsed eddy current thermography," *IEEE Sensors J.*, vol. 11, no. 12, pp. 3261–3268, Dec. 2011.

[14] X. Maldague and S. Marinetti, "Pulse phase infrared thermography," *J. Appl. Phys.*, vol. 79, no. 5, pp. 2694-1–2694-5, 1996.

[15] K. Chatterjee and S. Tuli, "Image enhancement in transient lock-in thermography through time series reconstruction and spatial slope correction," *IEEE Trans. Instrum. Meas.*, vol. 61, no. 4, pp. 1079–1089, Apr. 2012.

[16] S. Marinetti, E. Grinzato, P. G. Bison, E. Bozzi, M. Chimenti, G. Pieri, and O. Salvetti, "Statistical analysis of IR thermographic sequences by PCA," *Infr. Phys. Technol.*, vol. 46, nos. 1–2, pp. 85–91, Dec. 2004.

[17] A. A. Khan, V. Vrabie, J. I. Mars, A. Girard, and G. D'Urso, "A source separation technique for processing of thermometric data from fiber-optic DTS measurement for water leakage identification in dikes," *IEEE Sensors J.*, vol. 8, no. 7, pp. 1118–1129, Jul. 2008.

[18] N. Rajic, "Principal component thermography for flaw contrast enhancement and flaw depth characterisation in composite structures," *Composite Struct.*, vol. 58, no. 4, pp. 521–528, Dec. 2002.

[19] A. Hyvarinen, J. Karhunen, and E. Oja, *Independent Component Analysis and Blind Source Separation*. New York, USA: Wiley, 2001.

[20] J. Vrana, M. Goldammer, J. Baumann, M. Rothenfusser, and W. Arnold, "Mechanisms and models for crack detection with induction thermography," in *Proc. AIP Conf.*, 2008, pp. 475–482.

[21] J. Wilson, G. Y. Tian, I. Z. Abidin, S. Yang, and D. Almond, "Modelling and evaluation of eddy current stimulated thermography," *Nondestruct. Test. Evaluat.*, vol. 25, no. 3, pp. 205–218, Jan. 2010.

[22] B. Gao, W. L. Woo, and S. S. Dlay, "Single channel source separation using EMD-subband variable regularized sparse features," *IEEE Trans. Audio, Speech Lang. Process.*, vol. 19, no. 4, pp. 961–976, May 2011.

[23] G. J. Jang and T. W. Lee, "A maximum likelihood approach to single channel source separation," *J. Mach. Learn. Res.*, vol. 4, no. 1, pp. 1365–1392, Jan. 2003.

[24] M. E. Davies and C. J. James, "Source separation using single channel ICA," *Signal Process.*, vol. 87, no. 8, pp. 1819–1832, Aug. 2007

[25] D. James and W. Kahan, "Accurate singular values of bidiagonal matrices," *Soc. Ind. Appl. Math. J. Sci. Stat. Comput.*, vol. 11, no. 5, pp. 873–912, 1990.

[26] T. Sakagami and S. Kubo, "Development of a new crack identification technique based on near-tip singular electrothermal field measured by lock-in infrared thermography," *ASME Int. J. Ser. A*, vol. 44, no. 4, pp. 528–534, 2001.

[27] A. Yin, B. Gao, G. Y. Tian, W. L. Woo, and K. J. Li, "Physical interpretation and separation of eddy current pulsed thermography," *J. Appl. Phys.*, vol. 113, no. 6, pp. 064101-1–064101-8, Feb. 2013.

Libing Bai received the B.S. degree from the University of Electronic Science and Technology of China, Chengdu, China, 2008, where he is currently pursuing the Ph.D. degree.

His current research interests include measurement and control technology and instrument.

Bin Gao (M'12) received the B.S. degree in communications and signal processing from Southwest Jiao Tong University, Shanhaiguan, China, in 2005, the M.Sc. degree in communications and signal processing (with Distinction) and the Ph.D. degree from Newcastle University, Newcastle upon Tyne, U.K., in 2011.

He is currently a Research Associate with Newcastle University. His current research interests include blind source separation, audio and image processing, machine learning, structured probabilistic modeling, signal processing in NDE.

Gui Yun Tian (M'01–SM'03) received the B.Sc. degree in metrology and instrumentation and the M.Sc. degree in precision engineering from the University of Sichuan, Chengdu, China, in 1985 and 1988, respectively, and the Ph.D. degree from the University of Derby, Derby, U.K., in 1998.

He was a Lecturer, Senior Lecturer, Reader, Professor, and Head of the Group of Systems Engineering, University of Huddersfield, Huddersfield, U.K., from 2000 to 2006, Since 2007, he has been based at Newcastle University, Newcastle upon Tyne, U.K., where he has been the Chair Professor in sensor technologies. Currently, he is also with the School of Automation Engineering, University of Electronic Science and Technology of China, Chengdu, China. He has coordinated several research projects from the Engineering and Physical Sciences Research Council, Royal Academy of Engineering and FP7, on top of this he also has good collaboration with leading industrial companies, such as Airbus, Rolls Royce, BP, nPower, and TWI.

Wai Lok Woo (SM'12) received the B.Eng. degree (First Class Hons.) in electrical and electronics engineering and the Ph.D. degree from the Newcastle University, Newcastle upon Tyne, U.K.

He is currently a Senior Lecturer with the School of Electrical, Electronics and Computer Engineering, Newcastle University. He has an extensive portfolio of relevant research supported by a variety of funding agencies. He has authored over 200 papers on these topics on various journals and international conference proceedings. His current research interests include mathematical theory and algorithms for nonlinear signal and image processing. This includes areas of blind source separation, machine learning, multidimensional signal processing, and signal/image deconvolution and restoration.

Dr. Woo was the recipient of the IEE Prize and the British Scholarship in 1998 to continue his research work. Currently, he serves on the editorial board of the many international signal processing journals.

Yuhua Cheng (M'11) is a Doctor of Measurement Techniques and Automation Devices. He is with the University of Electronic Science and Technology of China, Chengdu, China, a technical school, and is also an Associate Professor with the Laboratory of Measurement and Control Technology and Instrument. His current research interests include nondestructive evaluation, structural health monitoring, and the application of photonics in sensing and communications systems.